

Ortho-para transitions in reactive $H^+ + H_2$ collisions

D. Gerlich

Fakultät für Physik, Universität Freiburg, D 7800 Freiburg, Germany

(Received 20 January 1989; accepted 2 November 1989)

An experimentally well-proven dynamically biased statistical theory is used to calculate state specific cross sections and product state distributions for the proton-hydrogen scrambling reaction. Conservation of parity and nuclear spin and the anisotropy of the interaction potential are explicitly taken into account. The influence of the permutation symmetry is explained with a simple statistical model. The results are used to calculate rate coefficients for state to state transitions, and for conversion of *ortho*- H_2 into *para*- H_2 . At low energies (< 43 meV), the decay of a $H^+ \cdot H_2(j=1)$ complex into the exothermic $H^+ + H_2(j=0)$ channel is strongly hindered, the probability is smaller than 1/12. Therefore, this $j=1$ to $j=0$ transition occurs with a rate coefficient of only 2.2×10^{-10} cm³/s at temperatures of interstellar space. A van't Hoff plot of the results shows that the *ortho-para* coupling via proton exchange leads to an equilibrium abundance ratio $n(\textit{ortho})/n(\textit{para}) = 9.35 \cdot \exp(-169.4 K/T)$. The concept of separate conservation of nuclear spin during the lifetime of the intermediate complex was tested experimentally in a high resolution molecular beam experiment. The partially resolved rovibrational distributions are in good agreement with populations calculated with the statistical model.

I. INTRODUCTION

The most abundant molecule in the universe H_2 exists in two nearly independent forms *ortho*- and *para*-hydrogen. At and above room temperature, the *p*- H_2 :*o*- H_2 equilibrium ratio is 1:3 (normal hydrogen) and it is assumed that this also holds for hydrogen molecules formed in exothermic reactions (e.g. ternary association), or via catalytic recombination of H atoms on the surface of grains.¹ In a low temperature environment, the separate even and odd rotational manifolds reach thermal equilibrium rather fast, but the rate of transformation between *o*- H_2 and *p*- H_2 is known to be very slow. This problem is of special interest under interstellar conditions where the thermal population is almost entirely shifted to *p*- H_2 . However, some doubt exists² as to whether the *ortho* to *para* coupling is effective enough to establish this overall low temperature thermodynamic equilibrium, or whether the *ortho* to *para* ratio of a given interstellar cloud depends on its chemical history and lifetime.

Different possible coupling mechanisms (radiative transitions, grain catalysis, neutral, and ionic gas phase reactions) have been discussed by several authors,³⁻⁵ and it has been concluded that the proton exchange $H^+ + H_2 \rightarrow H^+ + H_2$ plays the key role in *ortho* to *para* conversion. Although this reaction belongs to the most simple and elementary ones, there exist only approximate estimates for the conversion rate coefficients. For example the rates for collisional deexcitation from $j=1$ to $j=0$ vary from 1×10^{-10} (Ref. 4) to 1×10^{-9} cm³/s (Ref. 5). Conversion rates for higher rotational states are even less well known and are usually derived from simplified statistical arguments and considerations of detailed balance.⁶

The importance of the state to state process $H^+ + H_2(j) \rightarrow H^+ + H_2(j')$ for the understanding of measured interstellar $H_2(j)$ column densities⁷ has been discussed recently.⁸ Some conclusions from the results of the

present calculations for models of diffuse interstellar clouds have already been drawn⁹ and the inclusion of our data resulted in significant modifications of the calculated $H_2(j=0)$ and $H_2(j=1)$ densities.¹⁰

It has been discussed by Quack¹¹ that the mixing of *ortho*- H_2 and *para*- H_2 in the H_3^+ collision complex is hindered by restrictions due to symmetry selection rules. This author deduces approximate correction factors for statistical calculations and he concludes that only 1/6 of the encounters of H^+ with *o*- H_2 can result in *p*- H_2 products. In a preliminary version of our calculation,¹² we have shown that at total energies below the $j'=2$ threshold this ratio declines further to 1/12.

In this paper, we present a detailed application of a dynamically biased statistical theory¹³⁻¹⁵ to these problems. This theory has already been proven reliable in comparison with different experiments performed on the H_3^+ collision system in several isotopic modifications. For example, it has been used to predict rovibrational populations of the HD products formed in the reaction¹⁶ $H^+ + D_2 \rightarrow D^+ + HD(v,j)$ and to calculate absolute integral cross sections and thermal rate coefficients for proton-deuteron exchange in $H^+ + D_2$ and $D^+ + H_2$ collisions.¹⁷

The following work focuses on the highly symmetric case of three identical H atoms: In Sec. II we describe briefly the dynamically biased statistical theory with special emphasis on the influence of conservation of parity and nuclear spin. Particular attention is also given to the effect of the anisotropy of the long-range potential. State specific integral cross sections, intrinsic (detailed) rate coefficients, and thermally averaged rate coefficients are discussed in Sec. III. More specific results like product state distributions are presented in Sec. IV and they are compared to experimentally determined rovibrational populations of H_2 products. Some concluding remarks are given in Sec. V.

II. DYNAMICALLY BIASED STATISTICAL MODEL

The main features of the statistical model used in the present calculation have already been reported¹³⁻¹⁷; some more details will be published elsewhere. The interrelation with other statistical theories is discussed in a recent review on "statistical methods in scattering" by Quack and Troe.¹⁸ Therefore we can restrict the general part of the theory to a short compilation of a few formulas. In somewhat more detail we will discuss two special aspects which are important for the present work: (1) due to the exchange symmetry of three identical particles in the H_3^+ system, the conservation of the total nuclear spin during the lifetime of the complex plays a very important role; (2) in order to calculate reliable complex formation probabilities at very low energies, it became necessary to account numerically for the influence of the anisotropic long-range potential on the j dependence of the $\text{H}^+ + \text{H}_2(j)$ scattering.

A. State to state cross sections

For the highly symmetric system $\text{H}^+ + \text{H}_2$, the integral state to state cross sections have been calculated using the following equation [cf. Eq. (44) in Ref. 11] and evaluating explicitly the sums over all quantum numbers:

$$\sigma_{jv \rightarrow j'v'}^E = \frac{\pi}{k^2(2j+1)} \sum_{l=0}^1 \sum_{J=0}^{J_m} \frac{2J+1}{N^{JE\Pi}} \sum_{l'=|J-j|}^{J+j} P_{l'jv'}^{JE\Pi} \times \sum_{l'=|J-j|}^{J+j} P_{l'j'v'}^{JE\Pi} g_{j'j'} \quad (1)$$

where $N^{JE\Pi}$ is the sum over all states which are in accord with conservation of total energy E , total angular momentum J , and parity Π :

$$N^{JE\Pi} = \sum_{v=0}^{v_m} \sum_{j=0}^{j_m} \sum_{l=|J-j|}^{J+j} P_{l'jv'}^{JE\Pi} g_{j'j'}. \quad (2)$$

The channel wave number is given by

$$k^2 = 2\mu E_T / \hbar^2, \quad (3)$$

where μ is the reduced mass, E_T the translational energy, E the total available energy, J the total angular momentum, and J_m its maximum. j is the rotational, v the vibrational quantum number of the diatom, and l the orbital angular momentum quantum number of the relative motion. Primes mark the corresponding values of the product channel. The overall parity Π is given by $(-1)^{l+j}$ and is conserved, so allowing only $l'j'$ combinations leading to even or odd sums $l'+j'$, respectively. The nuclear spin degeneracy factors $g_{j'j'}$ and the complex formation probabilities $P_{l'jv'}^{JE\Pi}$ will be discussed in more detail below.

B. Nuclear spin statistical weights $g_{j'j'}$

The treatment of nuclear spin and symmetry properties within a statistical theory has already been discussed by several authors.^{11,18,19} Often, e.g., if a large number of channels is involved, it is sufficient to account for their effects only in the average, while in the present calculation the rotational transitions must be weighted individually with statistical factors $g_{j'j'}$. These factors have different values depending on how the total nuclear spin interacts with the other degrees of

freedom during the lifetime of the complex. We treat this problem in the following two extreme cases¹⁹:

(i) Coupled nuclear spin (CNS) approximation. If the nuclear spins are presumed to couple strongly with the other angular momenta, the degeneracy factors for *ortho*- H_2 and *para*- H_2 are only depending on the final rotational state j' ,

$$\text{CNS: } g_{j'j'} = \begin{cases} 3 & \text{if } j' \text{ odd} \\ 1 & \text{if } j' \text{ even.} \end{cases} \quad (4)$$

(ii) Frozen nuclear spin (FNS) approximation. If the total nuclear spin is conserved separately, the final state distribution becomes dependent on the initial state. For the detailed discussion of the corresponding statistical factor see Ref. 11. Briefly, one can derive this factor by considering that a complex with the total nuclear spin $I_T = 3/2$ can be formed only from and decay only to *ortho*- H_2 ($I = 1$), while only complexes with $I_T = 1/2$ allow for a transition between *ortho*- H_2 and *para*- H_2 . Conservation of total nuclear spin during the lifetime of the complex is therefore accounted for with

$$\text{FNS: } g_{j'j'} = \begin{cases} 5 & \text{if } j \text{ and } j' \text{ are odd} \\ 1 & \text{else.} \end{cases} \quad (5)$$

In general, these two ways to treat the nuclear spin result in only minor differences in measurable quantities¹⁹ like averaged total cross sections or rate coefficients. However, we have shown experimentally²⁰ for the rotationally state selected $\text{C}^+ + \text{H}_2$ ($j = 0$ or 1) collision system that one obtains measurable differences in the CH^+ production and it is obvious that spin effects play a dominant role in processes which include *ortho-para* conversion. It has been discussed¹¹ and proven in experiments^{12,20} that it is rather safe to assume that the lifetime of the complex is usually too short to change the nuclear spin I_T . Therefore, in most of our calculations the total nuclear spin has been treated as an additional good quantum number of the complex. In order to discuss the consequences of this assumption, some of the results have been calculated within the CNS approximation as well.

C. Complex formation probabilities

Following a rather general formulation of statistical theories given by Miller,²¹ the complex formation probabilities in Eq. (1) can vary smoothly between 0 and 1. In this way, the model takes into account that the transition from an initial state i ($= JE\Pi l v j$) into a final state f ($= JE\Pi l' v' j'$) can occur both directly and via formation of an intermediate complex c ($= JE\Pi$), allowing dynamical structure to be incorporated into the statistical model. For the direct part, we assume the validity of $P_{if}^0 = \delta_{ii} \cdot (1 - P_{ic})$, i.e., only the elastic process may take place directly, all other processes proceed through the complex. It seems to be worthwhile to mention here that in Eq. (1) the overall transition probability for those transitions which proceed via complex formation are parametrized exclusively in terms of the probabilities for complex formation P_{ic} . In this way, microscopic reversibility is preserved automatically.

In order to obtain a most realistic statistical model for the description of $\text{H}^+ + \text{H}_2$ collisions over an energy range

from meV to eV, we have examined in this study three different dynamical criteria for the determination of the complex formation probabilities:

L, Langevin model²²;

MDB, "most dynamically biased" statistical theory¹³⁻¹⁷;

TC, trajectory based capture.^{23,24}

These criteria have been applied to three different representations of the H_3^+ potential energy surface:

POL, polarization potential;

PQ, polarization and quadrupole potential;

DIM, diatomics-in-molecules potential.

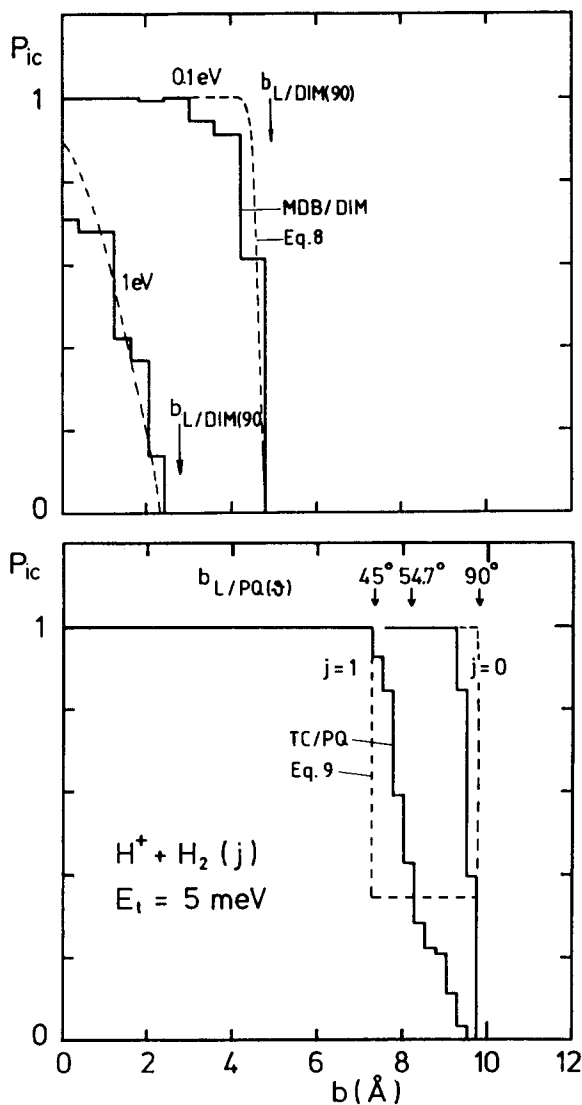


FIG. 1. Complex formation probabilities P_{ic} as a function of impact parameter. (a) The histograms are results from the MDB/DIM theory for the two collision energies $E_T = 1$ and 0.1 eV, the dashed lines represent the corresponding analytical fits, given by Eq. (8). $b_{L/DIM(90^\circ)}$ is the Langevin capture impact parameter calculated for the DIM potential at fixed orientation. (b) The histograms have been calculated with the trajectory capture method TC/PQ (collision energy, 5 meV; initial rotational states; $j = 0$ and 1). The dashed lines represent the analytical approximation, given by Eq. (9). The arrows mark the angle-dependent capture impact parameters $b_{L/PQ(\vartheta)}$ determined with the Langevin prescription on the PQ potential. $b_{L/PQ(54.7^\circ)}$ is identical with $b_{L/POL}$ because the quadrupole term vanishes for this orientation.

Results, presented in the figures and discussed in this chapter, are labeled with these acronyms according to method/potential.

The simplest dynamical criterion, the Langevin prescription, is based on capture behind the centrifugal barrier. It has been evaluated for the POL potential (leading to the usual Langevin model) and for the DIM and PQ potential at fixed orientations. These results are used only for comparison or as a reference standard. For example, the arrows in Fig. 1(a) mark the critical impact parameters $b_{L/DIM(90^\circ)}$ for the collision energies 0.1 and 1 eV while, in Fig. 1(b), $b_{L/PQ(\vartheta)}$ is shown for the fixed orientations $\vartheta = 45^\circ, 54.7^\circ$, and 90° . The energy-independent capture rate coefficient $k_{L/POL}$ is indicated in Fig. 2 as a dotted line, $k_{L/DIM(90^\circ)}$ as a dash-dotted line.

The MDB statistical theory has been discussed already in several aspects elsewhere.¹³⁻¹⁷ Briefly, trajectory calculations performed on a DIM-potential surface have been used to decide which of the initial conditions lead to a strongly coupled complex. As usual it has been required that the minimum of the three distances among the nuclei A , B , and C , i.e., $\min(R_{AB}, R_{AC}, R_{BC})$ changes at least eight times from one R_{ik} to another one. For an interval of initial conditions, the complex formation probability is defined as the fraction of trajectories fulfilling this requirement. Two examples are plotted in Fig. 1(a) as a function of the impact parameter b . The histograms illustrate that, only at low collision energies (below 0.2 eV), the MDB complex formation probability $P_{ic}(b)$ becomes similar to a step function, falling from one to zero very close to $b_{L/DIM(90^\circ)}$.

Integration over the impact parameter leads to complex formation cross sections $\sigma_{MDB/DIM}$, respectively, to intrinsic complex formation rate coefficient $k_{MDB/DIM} = (2E_T/\mu)^{1/2} \cdot \sigma_{MDB/DIM}$ (not thermally averaged). A few corresponding

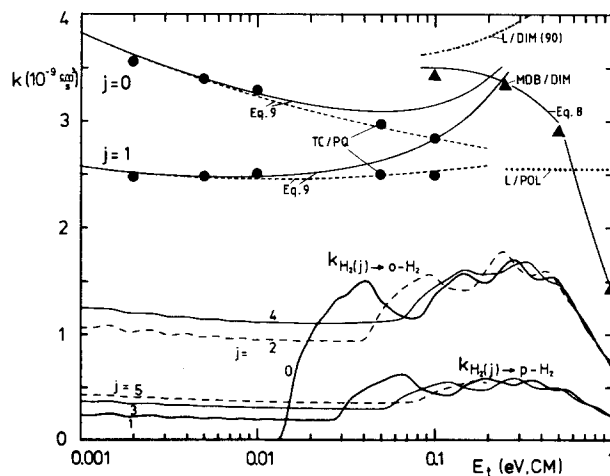


FIG. 2. In the upper part, various capture rate coefficients are plotted vs collision energy. The TC/PQ results (dots) are approximated by the analytical function given by Eq. (9) (dashed lines, solid lines—inclusion of the correction term $25 \cdot E_T^{1.3}$). The MDB/DIM results (triangles) are fitted by Eq. (8) (solid line). $k_{L/DIM(90^\circ)}$ (dash-dotted line) and $k_{L/POL}$ (dotted line) are capture rates according to the simple Langevin prescription. The curves in the lower half of the figure illustrate, that rate coefficients for state specific reactions (in this case, $k_j = \text{even} \rightarrow o\text{-H}_2$, and $k_j = \text{odd} \rightarrow p\text{-H}_2$) are only a fraction of the capture rate coefficients. The details of these results are discussed in Sec. III.

results are shown in Fig. 2 as triangles. Comparison of these data with $k_{L/DIM(90^\circ)}$ reveals that the MDB model and the simple capture model approach each other at energies below 0.2 eV.

In order to obtain more realistic complex formation probabilities at collision energies below 0.2 eV, we have performed additional calculations using a PQ (polarization and quadrupole) potential. This became necessary because the results of the MDB theory are based on a DIM-potential surface which has an incorrect long-range behavior: it has an exponential R dependence and has nearly spherical symmetry while the PQ potential has an R^{-4} and R^{-3} dependence and has an up to 3.8 meV high orientation-dependent barrier.

In such situations, it is common to use averaging procedures for the determination of reaction rate coefficients [e.g., average-dipole-orientation (ADO) or average-quadrupole-orientation (AQO) theory, or adiabatic approximations²³]. Our main interest, however, was to determine numerically precise cross sections, especially for the two lowest rotational states of H_2 . Therefore, also in this case, the complex formation probabilities have been determined via trajectory calculations.²⁴ Since below 0.2 eV "capture" in the sense of the Langevin model and "strong coupling" according to the MDB model are practically equivalent, it was sufficient to determine only capture probabilities. Several bunches of trajectories have been calculated²⁴ between 2 and 100 meV and for $j = 0$ and 1. The impact parameter-dependent capture probabilities have been extracted in the usual way.

Figure 1(b) shows some typical results as histograms. It is interesting to compare the position of the steep decrease of these functions with the capture impact parameters $b_{L/PQ(\vartheta)}$ calculated for fixed orientations. It is evident, that at this low energy (5 meV), the nonrotating target molecule ($j = 0$) has a tendency to adjust its orientation almost entirely into the minimum of the potential energy surface ($\vartheta = 90^\circ$). As a consequence, the resulting capture rate coefficients $k_{TC/PQ}$ ($j = 0$) (uppermost dots in Fig. 2) are larger than that based on the polarization potential alone and they increase with falling energy due to the R^{-3} dependence of the quadrupole term in the PQ potential.

For $j = 1$, the rotation is already fast enough that this orientation effect begins to vanish. The capture probability [Fig. 1(b)] drops slowly from 1 to 0 in an impact parameter interval ranging from $b_{L/PQ(45^\circ)}$ to $b_{L/PQ(90^\circ)}$. The resulting complex formation rate coefficients $k_{TC/PQ}$ ($j = 1$) (Fig. 2 dots) are almost energy independent and its magnitude is very close to the usual Langevin rate $k_{L/POL}$, although the opacity functions $P_{ic}(b)$ are somewhat different.

D. Analytical representation of P_{ic}

The trajectory based complex formation probabilities have been calculated for a large representative set of initial conditions. For the necessary interpolation and extrapolation, and also for easy numerical processing, it has been assumed that they are smooth functions of their index parameters. Inspection of the results has shown that one obtains a

satisfying description of the complex formation probability with the ansatz

$$P_{ic} = A(E, E_T, \mu) \cdot f(l, E_T, \mu). \quad (6)$$

The function $A(E, E_T, \mu)$ accounts for deviations between capture in the sense of the Langevin model and strong coupling according to the MDB model, while the function $f(l, E_T, \mu)$ describes mainly the dependence of the complex formation probability on the orbital angular momentum. Internal excitation of the molecule (vibration or rotation) enters only via the total energy E in the function $A(E, E_T, \mu)$. For $H^+ + D_2$ collisions, this analytical ansatz has been reported elsewhere,¹⁷ more details on the MDB statistical theory for isotopic variants of the H_3^+ system will be given in a separate publication.

With function (6), the three different models (L/POL, MDB/DIM, TC/PQ) can be approximated as follows: For the Langevin model, we obtain the usual 1-0 step function

$$f(l, E_T, \mu) = \begin{cases} 1 & \text{if } l \leq l_m \\ 0 & \text{else;} \end{cases}$$

for L/POL,

$$l_m = \{2567.68 \mu (\alpha E_T)^{1/2}\}^{1/2}, \quad (7)$$

$$A(E, E_T, \mu) = 1$$

(units are eV and atomic mass units u , α is the polarizability in \AA^3).

The MDB results have been approximated using

$$f(l, E_T, \mu) = \begin{cases} 1 - \exp\{(l - l_m)/l_s\} & \text{if } l \leq l_m \\ 0, & \text{else,} \end{cases}$$

MDB/DIM results have been extrapolated using

$$l_m = \min \begin{cases} 59 \mu^{1/2} E_T^{0.28} \\ 60 \mu, \end{cases} \quad (8)$$

$$A(E, E_T, \mu) = f(l = 0, E) / f(l = 0, E_T).$$

The trajectory data, obtained with the PQ potential, are approximated with the two parameters l_0 and l_1 (concerning the term $\{ + 25 E_T^{1.3} \}$ see below):

TC/PQ,

$$f(l, E_T, \mu) = \begin{cases} 1 & \text{if } l \leq l_1 \text{ or } (l \leq l_0 \text{ and } j = 0) \\ 1/3 & \text{if } l_1 < l \leq l_0 \text{ and } j > 0 \\ 0 & \text{if } l > l_0, \end{cases} \quad (9)$$

$$l_0 = 38.2 E_T^{0.235} \{ + 25 E_T^{1.3} \},$$

$$l_1 = 40.5 E_T^{0.3} \{ + 25 E_T^{1.3} \},$$

$$A(E, E_T, \mu) = 1.$$

Comparison between the trajectory based complex formation probabilities (histograms) or rate coefficients (triangles and dots) and their analytical representation can be made in Figs. 1 and 2. Figure 1(a) shows that, at a collision energy of 1 eV, the analytical function $P_{ic}(b)$ falls off very steeply in satisfying agreement with the trajectory data while, at 0.1 eV, it becomes very close to the 1-0 step function of the Langevin model.

Equation (9) makes use of this observation but accounts in addition for the j dependence of the capture process. Figure 1(b) shows that for $j = 0$ the numerical data are

well approximated by a function with a single step. The arrows in the upper part of Fig. 1(b) indicate that the maximum impact parameter (respectively, orbital angular momentum) is very close to the capture value, obtained with a cut through the PQ potential at $\vartheta = 90^\circ$. The approximation for $j \geq 1$ uses a two-step function and is based on the model that 1/3 of the collisions occur in a favorable orientation, while 2/3 see a less attractive potential cut. With increasing energy, the two limits l_0 and l_1 approach each other. This becomes evident in Fig. 2, where the numerical exact complex formation cross sections (dots) are compared with the corresponding analytical results ($k_{TC/PQ}$, dotted lines).

In order to obtain a most realistic statistical theory for comparison with experiments or for interstellar models and in order to cover the whole energy range from 1 meV to 1 eV with one model, it was necessary to interpolate smoothly between the TC/PQ and the MDB/DIM models. For this purpose, Eq. (9) has been modified slightly by adding the $25 \cdot E_T^{1.3}$ term in the definition of l_0 and l_1 . In practice, this correction accounts for the fact that at shorter distances ($R < 4 \text{ \AA}$) the realistic interaction potential is more attractive than the pure PQ long-range part. The influence of this correction on the capture rate coefficient can be seen in Fig. 2 by comparing the dotted and the solid lines for $k_{TC/PQ}$. All the following results have been obtained by using Eq. (9) in the modified version (i.e., with the additional term in brackets) at collision energies below 0.22 eV, and Eq. (8) above 0.22 eV and we will refer to this method using the acronym MDB/TC.

III. RESULTS

A. Integral cross sections, intrinsic rate coefficients

The dynamically biased MDB/TC model described in the last chapter has been used to calculate integral state to state cross sections at collision energies E_T between 1 meV and 1 eV using 128 sample points equidistantly spaced on a logarithmic energy scale. Both the initial and final rotational states have been varied between 0 and 9, resulting in a large data set of state to state cross sections $\sigma_{j \rightarrow j'}(E_T)$. Figure 3 shows some of these results for $\Delta j = j' - j = \pm 1$ transitions plotted as intrinsic rate coefficients $k_{j \rightarrow j'} = (2 \cdot E_T / \mu)^{1/2} \cdot \sigma_{j \rightarrow j'}(E_T)$.

The endothermic channels [Fig. 3(a)] rise very steeply from their thresholds up to a maximum. The following decrease is partly due to the onset of competitive channels, partly to the falloff of the complex formation cross section (Fig. 2). The most prominent rate coefficient is the $0 \rightarrow 1$ transition, leading to a very efficient conversion of *p*-H₂ ($j = 0$) into *o*-H₂ ($j = 1$) already at rather low energies ($k = 1.5 \times 10^{-9} \text{ cm}^3/\text{s}$ at $E_T = 40 \text{ meV}$).

The rate coefficients for the exothermic $\Delta j = 1$ channels [Fig. 3(b)] have a very weak energy dependence up to those energies, where additional transitions begin to compete with the $\Delta j = 1$ one. For the low temperature *ortho-para* coupling, it is important to note that the formation of H₂ ($j = 1$) from $j = 2$ is the most efficient process ($k = 1 \times 10^{-9} \text{ cm}^3/\text{s}$), while the $1 \rightarrow 0$ transition has the smallest rate coefficient and decreases monotonically from $2.5 \times 10^{-10} \text{ cm}^3/\text{s}$

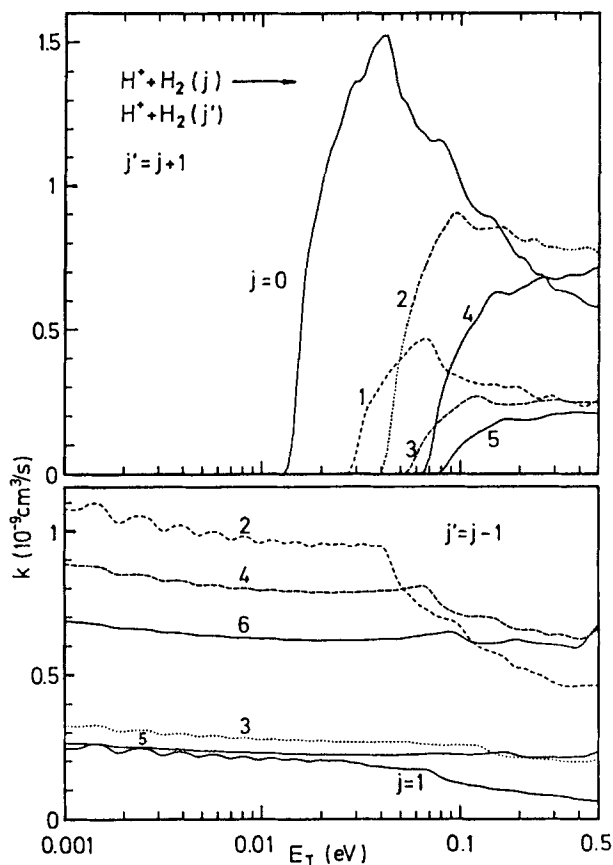


FIG. 3. Intrinsic rate coefficients for $\Delta j = \pm 1$ transitions. The endothermic transitions ($\Delta j = +1$) rise very steeply at their thresholds, while the exothermic transitions ($\Delta j = -1$) decrease monotonously. Population of the $j = 1$ state from $j = 2$ has the largest rate coefficient, while depopulation of $j = 1$ has the smallest value.

to below $1 \times 10^{-10} \text{ cm}^3/\text{s}$ in the energy range shown.

By summing over the corresponding final rotational states, intrinsic rate coefficients for the conversion of H₂ with specified initial odd rotational states into *para* hydrogen as well as conversion of H₂ (j even) into *o*-H₂ have been calculated. Some typical results are shown in the lower half of Fig. 2. At low energies, the curves are identical with those of Fig. 3, while above 40 meV one obtains a mean value of $5 \times 10^{-10} \text{ cm}^3/\text{s}$ (respectively, $1.5 \times 10^{-9} \text{ cm}^3/\text{s}$) with an oscillatory structure. This is due to the alternating growth of the *p*-H₂ and *o*-H₂ phase space with increasing energy and will be explained in more detail in Sec. III C and Fig. 6. The weak undulation below 10 meV (Fig. 3) is caused both by the discrete treatment of the orbital angular momenta in Eq. (1) and by the conservation of parity Π . At low energies, only a very few partial waves contribute to complex formation [e.g. from Eq. (9) follows $l_0(1 \text{ meV}) = 7$, $l_1(1 \text{ meV}) = 5$].

All the results presented so far have been calculated in the FNS approximation which is most probably realistic for our applications. However, in order to demonstrate the changes, calculations have been performed also in the CNS approximation. In addition, the L/POL model [Eq. (7), corresponding to the usual phase space theory] has been evaluated in a few cases as a reference. Some of the obtained

TABLE I. Elementary rate coefficients for conversion of $H_2(j=1)$ into $H_2(j=0)$ via proton exchange in units $10^{-10} \text{ cm}^3/\text{s}$. k_c is the complex formation rate coefficient. The frozen nuclear spin approximation (FNS) and the conservation of parity reduces the conversion efficiency in comparison to the CNS calculation. The L/POL model (corresponding to the usual phase space theory) predicts 15%–20% smaller values than the MDB/CT theory.

E_T	MDB/TC			L/POL		
	k_c	FNS	CNS	k_c	FNS	CNS
1 meV	26.0	2.43	3.91	25.5	2.01	3.26
25 meV	25.6	2.01	3.28	25.5	1.72	2.82

intrinsic rate coefficients for the conversion of $H_2(j=1)$ into $H_2(j=0)$ are presented in Table I for the two collision energies 1 and 25 meV. The capture rates $k_{L/POL}$ and $k_{TC/PQ}$ (see also Fig. 1) are almost identical. Comparison of the FNS and CNS values for $k_{1 \rightarrow 0}$ reveals that strong coupling of the nuclear spin to the other degrees of freedom leads to a significant increase of the rate coefficient by more than 60%. The MDB/TC theory predicts larger values for $k_{1 \rightarrow 0}$ than the L/POL theory because the $H^+ + H_2(j=0)$ channel has a larger phase space due to the anisotropy of the PQ potential. The thermal rate coefficients in the following section have been calculated exclusively with the MDB/TC model in the FNS approximation.

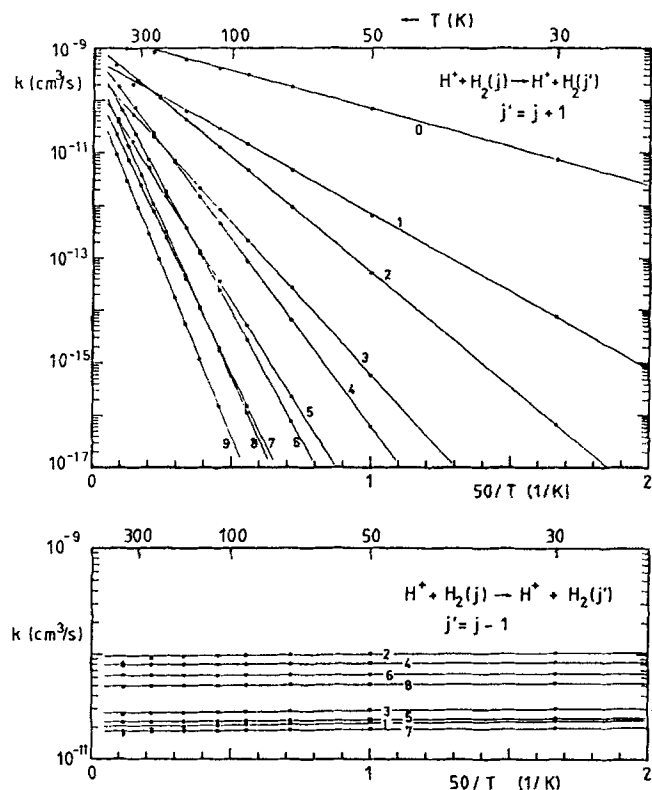


FIG. 4. The van't Hoff plot of thermal state to state rate coefficients. The dots have been calculated by numerical integration of the $\sigma_{j \rightarrow j'}$ over a Maxwell-Boltzmann distribution of the relative velocities. The lines are an Arrhenius type fit [see Eq. (10) and Table II].

B. Thermal rate coefficients

Thermal state to state rate coefficients have been calculated from $\sigma_{j \rightarrow j'}(E_T)$ by numerical integration over a thermal distribution of translational energies and varying the temperature from 10 to 500 K. Figure 4 illustrates that in a van't Hoff plot [logarithm of $k(T)$ vs $1/T$] the data points fall on a straight line. Therefore, for easy use of our results in reaction models (e.g., of interstellar space) the calculated thermal state to state rate coefficients have been approximated by

$$k_{j \rightarrow j'}(T) = k_0 \cdot \exp(-\Delta E_0/kT). \quad (10)$$

The parameters k_0 and ΔE_0 are given in Table II for all $j \rightarrow j'$ combinations up to $j' = j = 9$. The straight lines in Fig. 4 give an impression of the accuracy of this Arrhenius type fit, only at higher temperatures the calculated points are somewhat below the analytical function. For the endothermic channels, the "activation energies" ΔE_0 differ by just a few percent from the endoergicities, calculated from the rotational levels of H_2 . For the exothermic Δj transitions, the numerically determined ΔE_0 values are slightly below zero, i.e., the rate coefficients increase very slowly with falling temperature. The main variations of the preexponential parameter k_0 can be explained with simple statistical arguments, however, there are some additional deviations, especially for low j (see Sec. III C).

By further averaging over thermal populations of solely even (respectively, solely odd) rotational states, we finally obtain thermal rate coefficients for conversion of thermalized *o*- H_2 into *p*- H_2 and vice versa. Some numerical values are given in Table III and they are also presented together with the equilibrium constants $K = k_{p \rightarrow o}/k_{o \rightarrow p}$ in Fig. 5 in a van't Hoff plot. At high temperatures K reaches the value 3, i.e. the "normal" *ortho* to *para* ratio is obtained, while below 100 K the temperature dependence of the equilibrium constant can be approximated (fitted between 30 and 70 K) by the analytical expression

$$K = 9.35 \cdot \exp(-169.4 K/T). \quad (11)$$

Below 100 K, only $j=0$ and $j=1$ compete with each other and it is therefore not surprising that the activation temperature is very close to the energy difference of these two rotational levels (equivalent to 169.9 K in our calculation). Also, the preexponential factor 9.35 is very close to the ratio of the statistical weights of the two states (spin and rotation).

C. Comparison with simple statistical models

For a discussion of the restrictions due to exchange symmetry and statistical factors, it is appropriate to separate the dynamical constraints of the different statistical models from the simple statistical factors by calculating branching ratios instead of absolute cross sections. As an example, Fig. 6 shows the energy dependence of the conversion probability of $H_2(j=1)$ into *p*- H_2 . The results of the L/POL model (traditional PST, dashed line) and of the MDB/TC theory (heavy line) are rather similar. The lowest value in the L/POL theory is close to $1/16 (= 1/(1 \cdot 1 + 3 \cdot 5))$ and it is reached just below the $j' = 2$ threshold. The anisotropy of

TABLE II. The numerical results $k_{j \rightarrow j'}$, calculated for $\text{H}^+ + \text{H}_2(j) \rightarrow \text{H}^+ + \text{H}_2(j')$ for a manifold of $j \rightarrow j'$ transitions, have been approximated according to Eq. (10). The parameters k_0 (in $10^{-10} \text{ cm}^3/\text{s}$) are given in the upper part of the table, the "activation" energies ΔE_0 (in meV) in the lower part.

$k_0 j'$ j	0	1	2	3	4	5	6	7	8	9
0	...	19.606	13.714	11.119	7.936	8.320	5.698	5.143
1	2.024	...	6.248	17.432	3.436	12.913	2.153	9.763	0.087	...
2	2.889	9.575	...	12.179	10.093	8.300	5.873	6.282	0.986	...
3	0.522	8.202	2.729	...	3.582	13.589	2.812	8.908	1.248	...
4	1.071	3.398	5.700	7.910	...	7.927	6.256	5.259	5.517	0.556
5	0.246	3.818	1.275	8.883	2.246	...	2.267	9.674	1.707	5.432
6	0.565	1.755	2.932	4.088	5.209	6.223	...	6.480	5.316	5.270
7	0.145	2.230	0.743	5.179	1.320	7.977	1.828	...	1.804	7.866
8	0.432	1.107	1.792	2.496	3.185	3.851	4.489	4.974	...	4.127
9	0.160	2.448	0.803	5.074	0.744	4.445	1.039	5.915

$\Delta E_0 j'$ j	0	1	2	3	4	5	6	7	8	9
0	...	14.4	43.3	87.5	142	215	293	390
1	-0.331	...	29.3	71.3	129	199	280	379	434	...
2	-0.171	-0.183	...	43.2	100	170	250	348	416	...
3	-0.268	-0.250	-0.249	...	57.4	128	213	304	405	...
4	-0.199	-0.176	-0.159	-0.147	...	70.6	152	246	358	444
5	-0.281	-0.255	-0.241	-0.223	-0.217	...	83.2	178	286	399
6	-0.203	-0.169	-0.156	-0.142	-0.124	-0.124	...	96.1	202	327
7	-0.254	-0.216	-0.207	-0.199	-0.189	-0.177	-0.193	...	109	226
8	0.349	-0.052	-0.120	-0.118	-0.115	-0.109	-0.101	-0.135	...	117
9	-0.159	-0.117	-0.144	-0.188	-0.060	-0.100	-0.098	-0.094

the potential and conservation of parity leads to a slightly larger transition probability in the MDB/TC theory, especially at collision energies below 1 meV.

The main features of the computed curve can be explained with the following simple considerations: In the FNS approximation, the intermediate H_3^+ complex can be characterized by the total nuclear spin I_T which can have the two values $I_T = 3/2$ or $I_T = 1/2$ with statistical weights 4 or 2, respectively. Complexes with $I_T = 3/2$ can only be formed from and decay to *ortho*- H_2 because the nuclear spin of H_2 must be 1:

$$P(I_T = 3/2 \rightarrow j = \text{odd}) = 1, \quad P(I_T = 3/2 \rightarrow j = \text{even}) = 0. \quad (12)$$

TABLE III. Thermal rate coefficients ($10^{-10} \text{ cm}^3/\text{s}$) for the interconversion of *para* and *ortho* hydrogen $K = k_{p \rightarrow o}/k_{o \rightarrow p}$ is the equilibrium constant (see also Fig. 4).

T	$k_{p \rightarrow o}$	$k_{o \rightarrow p}$	K	Equation (11)
10	0.0000	2.078	0.0000	0.0000
30	0.0741	2.246	0.0330	0.0329
50	0.6842	2.243	0.3049	0.3158
70	1.850	2.224	0.8316	0.8314
90	3.255	2.274	1.431	1.423
110	4.509	2.398	1.879	2.004
130	5.845	2.539	2.301	2.540
150	6.968	2.667	2.612	...
170	7.756	2.855	2.716	...
190	8.481	3.056	2.774	...
210	9.038	3.194	2.829	...
230	9.632	3.259	2.955	...
250	9.902	3.445	2.873	...
270	10.28	3.563	2.887	...
290	10.65	3.652	2.918	...
310	10.89	3.736	2.915	...

Complexes with $I_T = 1/2$ can decay both to *p*- H_2 and *o*- H_2 . The branching ratio can be estimated simply from the statistical weights of the energetically accessible rotational states and one obtains for the formation of *o*- H_2 ,

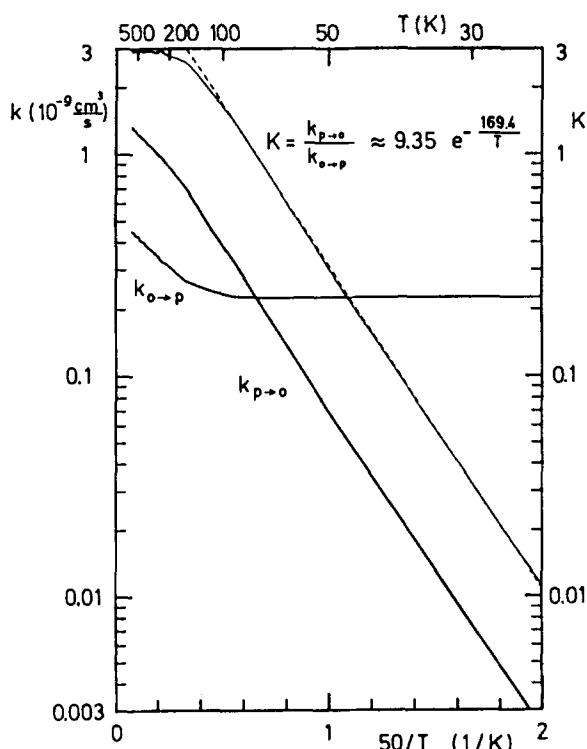


FIG. 5. van't Hoff plots of the thermal rate coefficients for *ortho-para* and *para-ortho* conversion in proton hydrogen collisions. Below 100 K, the derived equilibrium constant $K = k_{p \rightarrow o}/k_{o \rightarrow p}$ can be approximated with the Arrhenius ansatz given in Eq. (11) (dashed line).

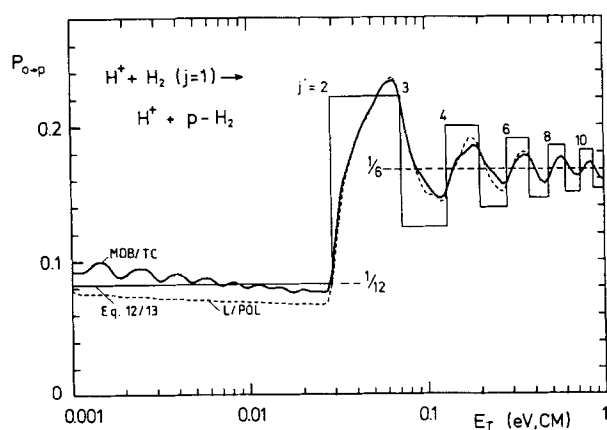


FIG. 6. The probability for converting $H_2(j=1)$ into *para* hydrogen as a function of the collision energy. Heavy line—MDB/TC theory; dashed line—phase space theory (L/POL). The step function is calculated from the transition probabilities, given in Eqs. (12) and (13).

$$P(I_T = 1/2 \rightarrow j: \text{even}) = \sum_{\text{even } j} (2j+1) / \sum_{\text{all } j} (2j+1). \quad (13)$$

If in a $H^+ + H_2(j=1)$ collision the intermediate complex is formed in the two I_T states according to their statistical weights (4/6 and 2/6), the overall probability for forming *p*- H_2 , can be calculated from Eqs. (12) and (13). Corresponding results are plotted in Fig. 6. The low energy limit is 1/12 because only $j=1$ and $j=0$ compete with each other [$P_{1 \rightarrow \text{para}} = (4/6 \cdot 0 + 2/6 \cdot 1/4)$]. With increasing collision energy, additional rotational states contribute and lead alternatively to an increase and a decrease of the relative statistical weight of the even states according to Eq. (13). The highest value of $P_{o \rightarrow p} = 2/9$ is obtained just below the threshold for the $j'=3$ state. At higher energies the transition probability converges to 1/6 because *o*- H_2 and *p*- H_2 occupy approximately the same phase space (disregarding nuclear spin). This value has been used already by Quack,¹¹ who derived approximate correction factors for data from statistical calculations which have been performed without accounting for symmetry or nuclear spin effects. Figure 6 corroborates that these factors are applicable if the number of states is sufficiently large.

Until recently it was common practice, e.g., in comprehensive models of interstellar clouds,⁸ to deduce the rate coefficients for the j -changing $H^+ + H_2$ collisions from the simple relation⁶

$$k_{j+2 \rightarrow j+1} / k_{j+1 \rightarrow j} = (2j+3) \cdot g_{j+1} / (2j+5) \cdot g_{j+2}, \quad (14)$$

where g_j is the nuclear statistical weight of state j , with $g_j = 3$ and 1 for *o*- H_2 and *p*- H_2 , respectively. For the $1 \rightarrow 0$ transition a value of $3 \times 10^{-10} \text{ cm}^3/\text{s}$ has been assumed.⁸ Table IV shows a comparison of the only weakly temperature dependent MDB/TC rate coefficients $k_{j+1 \rightarrow j}$ with those calculated from Eq. (14). There are not only deviations concerning the overall absolute values, but also the scaling of Eq. (14) fails, especially for low rotational states. It has been shown in recent model calculations¹⁰ by Roueff that these differences lead to significant changes in the interpretation of column densities of interstellar hydrogen measured for the first eight rotational states.⁷

TABLE IV. Comparison of some thermal MDB/TC rate coefficients ($10^{-10} \text{ cm}^3/\text{s}$) for $\Delta j = -1$ transitions with those derived from simple statistical considerations. Equation (15) is in good overall agreement with the MDB/TC results if one chooses $k_c = 29.5 \times 10^{-10} \text{ cm}^3/\text{s}$. The usually used model (Refs. 6 and 8) [Eq. (14) with $k_{1 \rightarrow 0} = 3 \times 10^{-10} \text{ cm}^3/\text{s}$] leads to significant deviations.

T	1→0	2→1	3→2	4→3	5→4	6→5
MDB/TC (30 K)	2.3	10.3	3.0	8.4	2.4	6.5
MDB/TC (90 K)	2.1	9.8	2.8	8.1	2.3	6.3
Equation (15)	1.8	9.8	2.6	8.3	2.2	6.6
Equation (14)	3.0	5.4	1.3	3.0	0.8	2.1

The chief cause for the failing of Eq. (14) is the use of inadequate statistical factors, and the neglecting of the restrictions, imposed by conservation of nuclear spin (FNS approximation). This can be seen from a very simple statistical model which assumes a j -independent rate coefficient k_c for the formation of a complex, and uses for the calculation of its decay probabilities just those statistical factors $g_{j'}$ $\cdot (2j'+1)$ which have been discussed in Sec. II B. In this way, $k_{j+1 \rightarrow j}$ can be written as

$$k_{j+1 \rightarrow j} / k_c = g_{j+1, j} \cdot (2j+1) \sum_{j'=0}^{j+1} [g_{j+1, j'} \cdot (2j'+1)]. \quad (15)$$

Using $g_{j'}$ in the FNS approximation (5), the resulting $k_{j+2 \rightarrow j+1} / k_{j+1 \rightarrow j}$ ratios are in much better agreement with the MDB/TC results than those predicted by Eq. (14). Some absolute rate coefficients (based on an assumed value $k_c = 29.5 \times 10^{-10} \text{ cm}^3/\text{s}$) are shown in Table IV. Comparison with the MDB/TC results reveals that the differences amount to less than 10%, with the exception of the $1 \rightarrow 0$ transition which is affected by the anisotropy of the potential (see also Table I).

IV. PRODUCT STATE DISTRIBUTIONS

According to our knowledge, there exists presently no experimental method which allows one to test directly the low energy state to state cross sections reported in the preceding sections. Although the fundamental concepts of the statistical model applied to isotopic substitutes of $H^+ + H_2$ has been found very successful in comparison with measured integral and differential cross sections¹⁶ and low temperature rate coefficients,¹⁷ it was desirable to perform a direct experimental test of the assumptions used for the highly symmetric H_3^+ system, especially the restrictions due to exchange symmetry. In this section, we compare calculated FNS and CNS product state populations $P(v', j')$ with measured energy loss distributions, obtained in a high resolution beam experiment.^{12,25} The results prove that the total nuclear spin is conserved separately during the lifetime of the complex.

A. Calculated rovibrational distributions

Rovibrational distributions of the H_2 products have been calculated from the state to state cross sections given in Eq. (1) and using

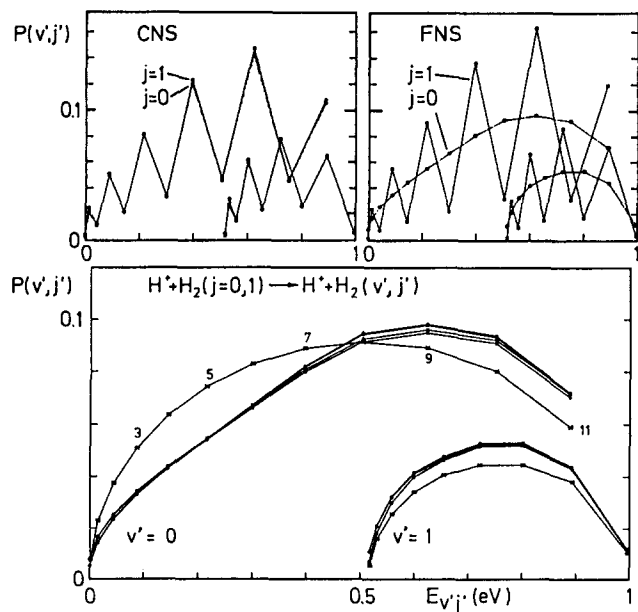


FIG. 7. Population probabilities of final rovibrational states (v', j') for proton-hydrogen scrambling collisions. The total energy of $E = 1$ eV allows one to excite rotational states up to $j' = 11$ for $v' = 0$, and $j' = 8$ for $v' = 1$. (a) The results of the CNS approximation show the 1:3 ratio of the even and odd states almost independent of whether the initial rotational state was 0 or 1. (b) The FNS approximation leads to a smooth distribution for $j = 0$, while for $j = 1$ the odd rotational states are strongly favored. (c) If one removes the odd-even structure in Figs. 7 (a) and 7(b) by using simple weighting factors (see the text) the resulting four distributions are practically indistinguishable. For comparison, the microcanonical equilibrium distribution is marked with stars.

$$P(v', j') = \sigma_{j_0 \rightarrow j' v'} / \sum_{j'' v''} \sigma_{j_0 \rightarrow j'' v''} \quad (16)$$

Some typical results are shown in Fig. 7 calculated for the two initial rotational states $j = 0$ and 1 for a total energy of 1 eV. In the CNS approximation [Fig. 7(a)], the two resulting distributions are almost indistinguishable, the insignificantly small differences are mainly due to the 14.4 meV smaller translational energy in the case of the $j = 1$ initial state. The assumed strong coupling of the nuclear spin leads to the high temperature *o*-H₂:*p*-H₂ ratio of 3:1 already after one single collision. In the FNS approximation [Fig. 7(b)], the populations are very different for the two initial states. One obtains a smooth distribution for $j = 0$, while for $j = 1$ the odd-even structure is even more pronounced than in Fig. 7(a).

For better comparison, the populations $P(v', j')$ of Figs. 7(a) and (b) have been weighted with simple statistical factors [odd rotational states 3/5 (CNS), respectively, 2/3 (FNS), even states 3 (CNS), respectively, 2 (FNS)]. These factors remove almost completely the even-odd structure as can be seen in Fig. 7(c), and lead to essentially identical curves. Again, this result is in accord with the already mentioned concept of an average statistical correction factor, proposed by Quack¹¹ and it shows that in the present case ($E = 1$ eV) the number of participating rovibrational states is sufficiently high to use them.

Comparison of the different statistical models (L/POL, MDB/TC) shows that the rovibrational distributions are

not very sensitive to the details of the theory, provided that the total energy exceeds a few tenths of an eV. Even the simple microcanonical equilibrium distribution $P_0(v', j')$ is rather similar as can be seen in Fig. 7(c). For reproducibility and to simplify matters, we preferred to use this reference distribution for analyzing the experimental data (see below) in the form

$$P_0(v', j') = \frac{1}{N} (2j' + 1) g_{j'} \cdot E_T'^{1/2}. \quad (17)$$

The normalization constant N is determined by $\sum P_0 = 1$. The translational energy after the collision E_T' can be calculated from the conservation of the total available energy $E = E_T + E_I - \Delta E_0 = E_I' + E_T'$. The reaction endoergicity ΔE_0 is zero in the present case and E_I is the internal energy (rovibration). The nuclear spin statistical weight $g_{j'}$ is defined in Eq. (4) or Eq. (5). In the FNS approximation, one obtains a microcanonical equilibrium distribution with "memory."¹¹

However, it must be mentioned that below $E = 0.2$ eV, where only a few rotational states are accessible, significant differences can occur between the MDB/TC result $P(v', j')$ and $P_0(v', j')$. For comparison, some numerical examples are given in Table V. The translational energy is fixed at $E_T = 0.1$ eV and the initial rotational states are varied between 0 and 3. For $j = 0$ and especially for $j = 1$, the MDB/TC theory (upper line) shows a very strong tendency to conserve the initial rotational state, while for $j \geq 2$ the two distributions are in reasonable agreement. Unfortunately both the energy range and the necessary energy resolution is out of the reach of the experiment described in the following section.

B. High resolution beam experiment

For comparison with the theoretical results, we have measured product internal state distributions in slow $H^+ + H_2$ collisions using our guided ion beam differential scattering apparatus. Details of this apparatus have been given in Ref. 16 and a short description can be found in Ref. 26. Briefly, the protons are created by electron bombardment in

TABLE V. Population of the rotational states ($j' = 0-4$) of H₂ products formed in $H^+ + H_2(j)$ reactions for several initial rotational states j . The collision energies is fixed at 0.1 eV. In each case, the upper line shows the results of the MDB/TC theory, while the lower line has been calculated from Eq. (17) (microcanonical equilibrium distribution). For the initial state $j = 0$, the results differ significantly, while the distributions for $j = 2$ and 3 are already in good agreement.

E_T	j	E_{tot}	j'				
			0	1	2	3	4
0.100	0	0.100	0.265	0.314	0.295	0.127	0
			0.100	0.277	0.374	0.249	0
0.100	1	0.114	0.043	0.507	0.124	0.326	0
			0.028	0.389	0.109	0.475	0
0.100	2	0.144	0.080	0.237	0.352	0.332	0
			0.081	0.229	0.336	0.354	0
0.100	3	0.187	0.018	0.273	0.089	0.535	0.086
			0.020	0.290	0.088	0.515	0.086

a rotatable storage ion source, and formed into a collimated (1°), pulsed ($1\text{--}2\ \mu\text{s}$), and slow ($0.5\text{--}2\ \text{eV}$) ion beam. The ions collide with the hydrogen target in a $l\text{-N}_2$ cooled scattering cell, which reduces the influence of the target motion,²⁷ and which restricts the rotational states to $j=0$ or $j=1$ only. The H_2 target gas has been used in the two *ortho-para* ratios 3:1 ($n\text{-H}_2$) and $\sim 1:3$ ("*p*"- H_2), which has been obtained by aging hydrogen in nitrogen ice ($48\text{--}50\ \text{K}$). The scattered products are analyzed by time of flight (TOF) in a 1 m long octopole ion beam guide. In the following results, the overall energy resolution was 70 meV, which is sufficient to obtain partially resolved rovibrational distributions. The laboratory scattering angle θ has been varied between 10° and 30° .

Measured TOF spectra have been transformed numeri-

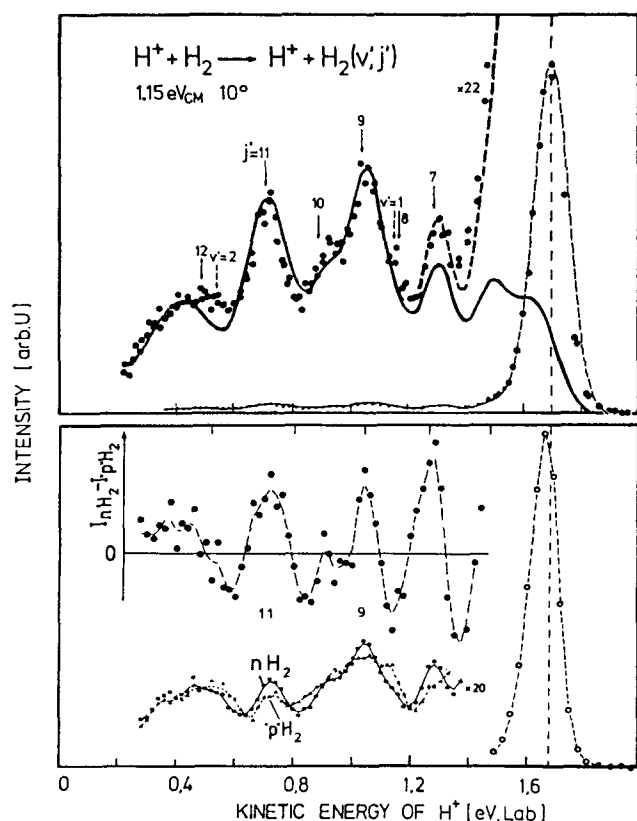


FIG. 8. Product kinetic energy distributions of scattered H^+ products, measured in a differential scattering apparatus at collision energy 1.15 eV, laboratory scattering angle 10° , and target temperature 80 K. The intense peak at about 1.6 eV (Lab) is produced by elastically scattered protons, the structure of the distributions at lower H^+ energies is due to excitation of discrete $\text{H}_2(v', j')$ states (see arrows in the blow up). (a) The upper part shows an experimental result (Refs. 16 and 26) obtained with $n\text{-H}_2$ as the target gas. The data are compared with a simulation based on the microcanonical equilibrium distribution [Eq. (17), heavy line]. For fitting the experimental dots below $j' \leq 7$ (dotted line), it was necessary to account in addition for direct elastic and inelastic scattering, the resulting $P_d(j')$ are given in Table VI. (b) The lower part shows results from another experiment (Refs. 12 and 25) performed with $n\text{-H}_2$ (25% $j=0$, 75% $j=1$, circles) and "*p*"- H_2 (76% $j=0$, 24% $j=1$, triangles) (here the lines are only guides for the eyes). In order to obtain reliable relative distributions, the target gas has been changed from $n\text{-H}_2$ to "*p*"- H_2 in many iterations. The nonvanishing difference $I_{n\text{-H}_2} - I_{p\text{-H}_2}$ points out that the nuclear spin is conserved during the lifetime of the complex.

TABLE VI. The experimental data in Fig. 8 have been fitted by using Eq. (17) for the statistical part of the distribution and the probabilities of this table for rotational excitation via direct elastic and inelastic collisions.

j'	0	1	2	3	4	5	6	7
$P_d(j')$	1.7	5.7	0.17	0.51	0.034	0.102	0.000	0.034

cally into lab-energy distributions. A typical example is shown in Fig. 8. A problem in the analysis of the data is that rearrangement competes with elastic and inelastic scattering. Especially at small scattering angles, directly scattered protons prevail over those products which emerge out of a strongly coupled complex. The magnified ($\times 22$) part of the spectrum shows contributions from all energetically accessible states. Experiments performed at larger scattering angles¹⁶ proved that the relative contribution of the direct part decreases rather fast, while the angle dependence of the remaining broad distribution changes as expected from the decay of a statistical complex. The peaks correspond to partially resolved rovibrational states marked by arrows. The dominance of odd over even rotational states is obvious.

As discussed above and due to the uncertainties caused by the contribution of directly scattered protons, we preferred to analyze the data simply with the microcanonical equilibrium distribution $P_0(v', j')$ defined in Eq. (17), and by adding empirically determined probabilities $P_d(j')$ for direct scattering as given in Table VI. For the simulation of the resulting experimental distributions measured at a given laboratory scattering angle, we assumed that the angular dependence of the differential cross section $d\sigma/d\omega$ is proportional $1/\sin \vartheta$, ϑ being the c.m. scattering angle. Allowing for the resolution of the apparatus,²⁷ one obtains finally the expected distributions. The example in Fig. 8(a) (dashed line) shows that this procedure allows us to fit nicely the experimental points. The solid line is based on the microcanonical equilibrium distribution alone and indicates that the population of $j=9\text{--}12$ is unaffected from directly scattered products and, therefore, can be used to test conservation of nuclear spin in the long-lived intermediate complex.

Since for $n\text{-H}_2$ as a target the *ortho-para* ratio remains unchanged regardless of whether the nuclear spin is treated in the FNS or CNS approximations, we have performed additional experiments^{12,25} with target gas prepared in the non-equilibrium ratio 76% $j=0$ and 24% $j=1$ ("*p*"- H_2). In order to obtain reliable relative distributions for the two different *ortho-para* compositions, it was necessary to change the target gas rather often (every half hour) and to average over many (up to 20) iterations under otherwise identical circumstances. Some typical results are shown in Fig. 8(b). The distribution obtained with "*p*"- H_2 (triangles) is clearly distinct from that obtained with $n\text{-H}_2$ (small dots), while the elastic peaks (only one is shown, circles) are practically identical. From the difference of the two distributions (upper half of the lower panel), it becomes obvious that there is some memory: scrambling collisions with H_2 in $j=1$ result in a nonstatistical preference of odd product states. If the coupling of the nuclear spin would be sufficiently strong, one would obtain two almost identical distributions as in Fig.

7(a), resulting in a vanishing difference.

It should be noted that the two n -H₂ examples in Figs. 8(a) and 8(b) are not comparable in the same way as the two curves in Fig. 8(b). Although they have been obtained under similar nominal conditions (collision energy, scattering angle) and with the same apparatus, they descend from very different runs (see Refs. 12, 16, 25, and 26). Many difficulties (e.g., surface potential distortions, changes in angular and energy resolution) complicate the reproducibility and for the determination of a reliable difference between n -H₂ and p -H₂, the experimental procedure described above is mandatory. The differences [as in Fig. 8(b)] are then reproducible within 20%.

A more detailed analysis of the difference between n -H₂ and " p "-H₂ has been performed by simulating the corresponding distributions. Figure 9 shows some results based on the microcanonical equilibrium distribution and using g_{ij} from Eq. (5). Under the conditions of our experiment, and provided that the FNS approximation is valid, the difference $I_{n-H_2} - 0.6 \times I_{p-H_2}$ corresponds to a population of pure odd rotational states. The resulting curve (heavy line in Fig. 9) is in very good agreement with the experimental dots which have been calculated from the two experimental curves using the same weighted difference. Similar experimental results²⁵ obtained at several energies (0.8–1.2 eV) and angles ($\theta = 10^\circ$ – 20°) corroborate the validity of the assumptions in this energy range. An estimate of the possible experimental uncertainties leads finally to $P(o \rightarrow p) = (1 \pm 0.2)/6$ in agreement with the assumption of conservation of nuclear spin.

V. CONCLUSIONS

Although the proton interchange in $H^+ + H_2$ collisions is one of the simplest prototypes of a reaction occurring be-

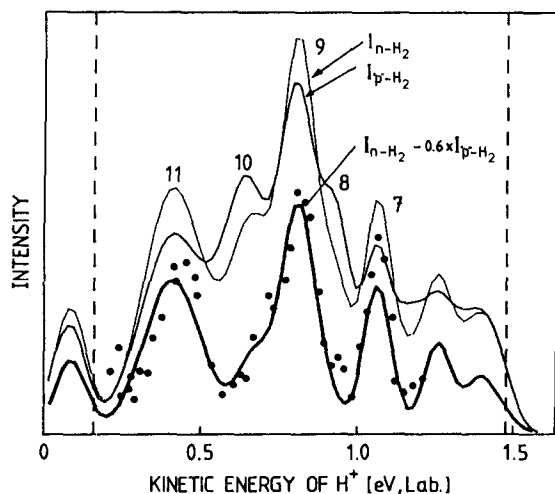


FIG. 9. Product kinetic energy distributions of scattered H^+ products (collision energy 0.98 eV, $\theta = 10^\circ$, target temperature 80 K). The two curves, marked with I_{n-H_2} and I_{p-H_2} , are the theoretical predictions [Eq. (17), FNS approximation] for the two different *ortho-para* mixtures used in the experiment. For a quantitative comparison, the weighted difference $I_{n-H_2} - 0.6 \times I_{p-H_2}$ is shown both for the experiment (dots) and the simulation (heavy line).

low 2 eV on a single potential energy surface via a strongly bound intermediate, and although it is probably the most abundant chemical reaction in the universe, detailed experimental or theoretical information is rather scarce at thermal energies. In the present work, we have applied a detailed statistical model to determine state to state cross sections and to extract thermal rate coefficients and product populations.

The dynamically biased statistical model has been developed initially for $H^+ + D_2$ and $D^+ + H_2$ reactions and the derived integral cross sections and rate coefficients have been found to be in agreement with measured values within the experimental uncertainties of typical 20%. In general, the same accuracy can be expected for the $H^+ + H_2$ system, however, in spite of the close similarities of the collision systems some precaution is advisable. On one side isotopic substitution causes additional perturbations,^{15,28} the energy levels are shifted, and the thermoneutral reaction becomes endo- or exothermic due to differences in zero point energy. On the other side, the exchange symmetry of three identical particles suppresses strong coupling between certain classes of states. Mixing requires now a magnetic moment acting on the spins of the nuclei. It has been shown experimentally²⁹ and theoretically³⁰ that even in collisions with paramagnetic substances the *ortho-para* conversion probability is extremely low (about 5×10^{-13} per collision, see also Ref. 31). Therefore it seems to be rather safe to assume the validity of the conservation of nuclear spin as long as the lifetime of the complexes is below the μ s range.

Summing up, we believe that the present results provide a reliable ($\pm 20\%$) data base for the inclusion of proton-hydrogen scrambling reactions in model calculations of chemical gas phase systems over a wide temperature range. However, at higher energies (> 1 eV), one has to expect deviations due to incomplete exchange between the incident proton and the hydrogen molecule, and one leaves the range of validity of our statistical model. It has been proven experimentally³² that at 3.7 eV c.m. even Δj transitions prevail in $H^+ + H_2$ collisions, a consequence of a direct collision mechanism.

ACKNOWLEDGMENTS

The author is indebted to Christoph Schlier for his continuous, stimulating interest, and grateful to Eveline Roueff for fruitful discussions and several hints. Many thanks are due to Hansjörg Bohli who helped in performing the scattering experiments. Support of our work by the Deutsche Forschungsgemeinschaft is acknowledged.

¹W. D. Watson, Rev. Mod. Phys. **48**, 513 (1976).

²D. R. Flower and G. D. Watt, Monthly Notes R. Astr. Soc. **209**, 25 (1984).

³D. E. Osterbrock, Astrophys. J. **136**, 359 (1962).

⁴A. Dalgarno, J. H. Black, and J. C. Weisheit, Astrophys. Lett. **14**, 77 (1973).

⁵R. R. Reeves and P. Harteck, Z. Naturforsch. Teil A **34**, 163 (1979).

- ⁶J. H. Black and A. Dalgarno, *Astrophys. J. Suppl. Ser.* **34**, 405 (1977).
- ⁷L. Spitzer and W. A. Morton, *Astrophys. J.* **204**, 731 (1976).
- ⁸Y. P. Viala, E. Roueff, and H. Abgrall, *Astron. Astrophys.* **190**, 315 (1987).
- ⁹E. Roueff, H. Abgrall, J. le Bourlot, and Y. Viala, in *Reactive Rate Coefficients in Astrophysics*, edited by D. Reidel (Manchester, 1987).
- ¹⁰D. Gerlich and E. Roueff, in *Symposium on Atomic and Surface Physics*, edited by A. Pesnelle, F. Gounand, M. Cheret, and F. Falve (CEN Saclay, La Plagne, 1988), p.93.
- ¹¹M. Quack, *Mol. Phys.* **34**, 477 (1977).
- ¹²D. Gerlich and H. Bohli, in *European Conference on Atomic Physics*, edited by J. Kowalski, G. zu Putlitz, and H. G. Weber (European Physical Society, Heidelberg, 1981), p. 930.
- ¹³D. Gerlich, U. Nowotny, Ch. Schlier, and E. Tely, *Chem. Phys.* **47**, 245 (1980).
- ¹⁴Ch. Schlier, in *Energy Storage and Redistribution in Molecules*, edited by J. Hinze (Plenum, New York, 1983).
- ¹⁵Ch. Schlier and U. Vix, *Chem. Phys.* **113**, 211 (1987).
- ¹⁶D. Gerlich, Ph.D. Thesis, University of Freiburg, 1977.
- ¹⁷D. Gerlich, in *Symposium on Atomic and Surface Physics*, edited by W. Lindinger, F. Howorka, T. D. Märk, and F. Egger (Institut für Atomphysik der Universität Innsbruck, Innsbruck, 1982) p. 304.
- ¹⁸M. Quack and J. Troe, in *Theoretical Chemistry*, edited by D. Henderson (Academic, New York, 1981), Vol. 6B, p. 199.
- ¹⁹A. F. Wagner and D. G. Truhlar, *J. Chem. Phys.* **57**, 4063, (1972).
- ²⁰D. Gerlich, R. Disch, and S. Scherbarth, *J. Chem. Phys.* **87**, 350 (1987).
- ²¹W. H. Miller, *J. Chem. Phys.* **52**, 543 (1970).
- ²²M. P. Langevin, *Ann. Chim. Phys. Ser. 8* **5**, 245 (1905).
- ²³K. Kern and Ch. Schlier, *Z. Phys. D* **1**, 391 (1986).
- ²⁴K. Kern, Diplom Thesis, University of Freiburg, 1985.
- ²⁵H. Bohli, Diplom Thesis, University of Freiburg, 1986.
- ²⁶E. Tely, in *Electronic and Atomic Collisions*, edited by G. Watel (North-Holland, Amsterdam, 1978), p. 591.
- ²⁷D. Gerlich, *J. Chem. Phys.* **90**, 127 (1988).
- ²⁸O. Brass and Ch. Schlier, *J. Chem. Phys.* **88**, 936, (1988).
- ²⁹L. Farkas and H. Sachse, *Z. Phys. Chem. B* **23**, 1, (1933).
- ³⁰E. Wigner, *Z. Phys. Chem. B* **23**, 28 (1933).
- ³¹G. Herzberg, *Spectra of Diatomic Molecules*, 2nd ed. (Van Nostrand, New York, 1950), p. 139.
- ³²K. Rudolph and J. P. Toennies, *J. Chem. Phys.* **65**, 4483 (1976).